Structure of the Substrate Binding Pocket of the Multidrug Transporter EmrE: Site-Directed Spin Labeling of Transmembrane Segment 1[†]

Hanane A. Koteiche, Matthew D. Reeves, and Hassane S. Mchaourab*

Department of Molecular Physiology and Biophysics, Vanderbilt University, Nashville, Tennessee 37232

Received February 20, 2003; Revised Manuscript Received April 1, 2003

ABSTRACT: Site-directed spin labeling (SDSL) was used to explore the structural framework responsible for the obligatory drug−proton exchange in the *Escherichia coli* multidrug transporter, EmrE. For this purpose, a nitroxide scan was carried out along a stretch of 26 residues that include transmembrane segment 1 (TMS1). This segment has been implicated in the catalytic mechanism of EmrE due to the presence of the highly conserved glutamate 14, a residue absolutely required for ligand binding. Sequence-specific variation in the accessibilities of the introduced nitroxides to molecular oxygen reveals a transmembrane helical conformation along TMS1. One face of the helix is in contact with the hydrocarbon interior of the detergent micelle while the other face appears to be solvated by an aqueous environment, resulting in significant exposure of the nitroxides along this face to NiEDDA. TMS1 from two different subunits are in close proximity near a 2-fold axis of symmetry as revealed by the analysis of spin−spin interactions at sites 14 and 18. The limited extent of spin−spin interactions is consistent with a scissor-like packing of the two TMS1. This results in a V-shaped chamber which is in contact with the aqueous phase near the N-terminus. The spatial organization of TMS1, particularly the close proximity of E14, is consistent with a proposed mechanistic model of EmrE [Yerushalmi, H., and Schuldiner, S. (2000) *Biochemistry 39*, 14711−14719] where substrate extrusion is coupled to proton influx through electrostatic interactions and shifts of the glutamate 14 pK_a during the cycle.

One of the mechanisms underlying multidrug resistance in organisms involves the extrusion of cytotoxic drugs via membrane embedded proteins, known as multidrug transporters (*1*). This class of transporters is characterized by a broad range of specificity, binding and extruding structurally dissimilar molecules in an energy-dependent process. While this mechanism is crucial for maintaining a healthy chemical composition inside the cell, it is a major problem in the treatment of tumor cells and infectious diseases. Multidrug transporters confer resistance to a variety of applied antibiotics and chemotherapeutic drugs, rendering them ineffective (*2*−*4*).

Bacterial multidrug transporters are divided into two major classes: the ABC[1] transporters (*5*), which use the free energy of ATP hydrolysis to pump toxins out of the cell, and the secondary multidrug transporters, which utilize the transmembrane electrochemical gradient of protons to power drug transport in an antiporter mechanism (*6*). Secondary multidrug transporters belong to four superfamilies, of which the small multidrug resistance (SMR or MiniTexans) family seems to be the simplest from a molecular perspective (*7*). The substrates of these pumps are chemically unrelated antiseptic and intercalating dyes. Substrate translocation is coupled to the influx of protons along their concentration gradient. EmrE, a secondary multidrug transporter from *Escherichia coli*, belongs to the SMR family (*8*). It is 110 amino acids long and is functional as an efflux pump that extrudes a variety of hydrophobic cations, such as tetraphenylphosphonium, methyl viologen, and ethidium bromide. EmrE is mostly hydrophobic with a total of eight charged residues. Only one of these residues, E14, a highly conserved residue in the SMR family, is embedded in the membrane. This residue has been shown to be critical in the binding and transport of substrates (*9*). EmrE has been purified and functionally reconstituted into proteoliposomes where it catalyzes cation−proton exchange, transporting one substrate molecule for two protons (*10*).

Hydropathy and α-periodicity analysis of EmrE predict the presence of four transmembrane helical segments, a model supported by NMR studies of EmrE solubilized in organic solvents (*11*−*13*). A cysteine scanning of various domains throughout the EmrE gene reveals that residues in the putative hydrophilic loops interact with *N*-ethylmaleimide while residues in the putative transmembrane domains have no accessibility to the reagent (*14*). This has been interpreted to suggest the lack of a hydrophilic translocation pathway. Early studies have shown that EmrE functions as an oligomer with a number of subunits between 2 and 4 (*15*). Recently, a cryo-EM projection structure of EmrE to 7 Å resolution

[†] This work was partly supported by a grant from the Center for Structural Biology at Vanderbilt University.

* Address correspondence to this author. E-mail: Hassane.mchaourab@vanderbilt.edu.

[1] Abbreviations: SDSL, site-directed spin labeling; EPR, electron paramagnetic resonance; TMS1, transmembrane segment 1; SMR, small multidrug resistance; ABC, ATP binding cassette; cryo-EM, cryo-electron microscopy; NMR, nuclear magnetic resonance; MTSSL, methanethiosulfonate spin label; DM, dodecyl maltoside; WT, wild type; WT*, cysteine-less wild type; VDW, van der Waals; SEC, size-exclusion chromatography; NiEDDA, nickel(II) ethylenediaminediacetate; SDS−PAGE, sodium dodecyl sulfate−polyacrylamide gel electrophoresis.

10.1021/bi0342867 CCC: $25.00
Published on Web 05/02/2003

has been interpreted as evidence of an asymmetric dimer (*16*).

Detailed information about the structural features and conformational changes that determine drug binding and transport by multidrug transporters is a critical step in the efforts to develop strategies to inhibit these transporters, with direct implications on chemotherapeutic and antibiotic treatments. Therefore, we have used site-directed spin labeling (*17*) to gain insight into the structure of the first transmembrane segment (TMS1) predicted to participate in substrate binding and to explore its involvement in oligomer formation. Residues 3 through 28 were replaced with cysteine, one at a time, in a cysteine-less background. The reactive sulfhydryl was then reacted with the highly specific methanethiosulfonate spin label (*18*). EPR analysis of the spin-labeled mutants reveals a helical conformation along TMS1. Furthermore, dipolar coupling between spin labels demonstrates that TMS1 from two subunits are in close proximity near an axis of 2-fold symmetry. The results are discussed in the context of a mechanistic model of substrate transport and energy transduction (*19*).

MATERIALS AND METHODS

Materials

Methanethiosulfonate spin label (MTSSL) was obtained from Toronto Research Chemicals; Ni-NTA media was obtained from Qiagen; Superdex 200 and HiTrap desalting columns were obtained from Amersham Biosciences; dodecyl maltoside (DM) was purchased from Anatrace; *E. coli* total lipid extract was purchased from Sigma; DNA oligonucleotides were purchased from IDT DNA; Bio-Beads were obtained from Bio-Rad.

Methods

Cloning and Site-Directed Mutagenesis. The cDNA of EmrE was amplified from *E. coli* MG1655 and cloned into the *Nde*I and *Hin*dIII sites of the plasmid pET20(b+). A spacer and a His_6 tag were added at the C-terminus to facilitate purification as previously described (*14*). The cloned DNA was sequenced and determined to be identical to the sequence deposited in GenBank under accession number P23895. To perform site-directed mutagenesis, four new unique restriction sites were introduced by silent substitutions in the nucleotide sequence. The EmrE gene codes for three native cysteines, which were mutated to serines without loss of function (*14*). Upstream mutagenic primers containing the desired X → cysteine substitution were used in conjunction with downstream primers to generate PCR fragments using cysteine-less EmrE as the template. The fragments were then digested and subcloned. For all of the mutants, the entire amplified region of the gene was sequenced to confirm the substitution and the absence of unwanted changes. Single cysteine mutants are named by specifying the original residue, the number of the residue, and the new residue, in that order.

Expression and Processing. Plasmids containing the single cysteine mutation were used to transform competent *E. coli* BL21(DE3). Overnight seeds were used to inoculate 1 L flasks of minimal media A (MMA) supplemented with glycerol (0.5%), thiamin (2.5 μg/mL), ampicillin (100 μg/mL), $MgSO_4$ (1 mM), and MEM amino acids 50× (1 mL).

Scheme 1

Cultures were grown at 37 °C until $OD_{600} \approx 1.2$; then the temperature was lowered to 33 °C and the expression of EmrE induced by the addition of 0.5 mM IPTG. After 3 h of induction, the cells were harvested by centrifugation and resuspended in lysis buffer (10 mM Tris-HCl, 250 mM sucrose, 150 mM choline chloride, 2.5 mM $MgSO_4$, 10 mM DTT, 15 μg/mL DNase, pH 7.5). The resuspended pellets were homogenized using the EmulsiFlex-C5 (Avestin). The lysates were then centrifuged at 10000*g* for 5 min to remove cell debris. The supernatants were centrifuged at 388000*g* for 1 h at 4 °C. The membrane pellet was resuspended in buffer containing 50 mM sodium phosphate, 300 mM NaCl, 10 mM imidazole, and 3 mM BME, pH 8.0, and solubilized by the addition of 1% dodecyl maltoside (DM) and stirring for 30 min at 4 °C. The solubilized membranes were centrifuged at 388000*g* for 1 h at 4 °C.

Purification, Labeling, and Reconstitution. The supernatant was collected and loaded on a Ni-NTA (Qiagen) column equilibrated in buffer A (50 mM sodium phosphate, 300 mM NaCl, 0.08% DM, pH 8), washed with buffer containing 30 mM imidazole, and eluted with buffer B containing 250 mM imidazole. The fractions collected were pooled and labeled with a 10-fold excess of the methanethiosulfonate spin label overnight at 4 °C (Scheme 1).

The labeled protein was then desalted by size-exclusion chromatography on a Superdex 200 column in SEC buffer containing 50 mM sodium phosphate, 300 mM NaCl, and 0.08% DM, pH 7.2. For reconstitution, the protein sample, desalted in a buffer with 0.04% DM, was mixed at 1:1000 molar ratio with a liposome solution and incubated at room temperature with gentle agitation for 30 min. The mixture was then diluted to 30 mL with reconstitution buffer containing 15 mM Tris-HCl and 150 mM NaCl, pH 7.5. Bio-Beads were then added to a total volume of 1 mL. The solution was incubated overnight at 4 °C. The Bio-Beads were allowed to settle, and the supernatant was centrifuged at 388000*g* for 1 h. The pellets were then resuspended in reconstitution buffer.

Ethidium Resistance Assay. The ability of the mutants to confer resistance to toxic compounds was tested as previously described (*14*). Briefly, overnight cultures of *E. coli* expressing mutant EmrE were grown to saturation. The cultures were then diluted 10-, 10^3-, and 10^6-fold, and 5 μL of the dilutions was plated on LB-amp plates containing 200 μg/mL ethidium bromide. Growth was examined after incubation at 37 °C for 24 h. Growth at the 10^3-fold dilution was interpreted to indicate a functional EmrE mutant.

Electron Paramagnetic Resonance Spectroscopy. The EPR spectra of spin-labeled EmrE mutants were obtained on a Bruker E500 spectrometer equipped with a superhigh Q cavity. Samples were prepared in SEC buffer and loaded in 25 μL glass capillary tubes. The microwave power was 5 mW incident, and the modulation amplitude was 1.6 G. Power saturation experiments were carried out on a Varian

spectrometer equipped with a loop-gap resonator. Samples were loaded in gas-permeable TPX capillaries, and the measurements were carried out under nitrogen and in the presence of 20% oxygen or 50 mM NiEDDA. The data were analyzed to obtain the parameter $P_{1/2}$. The EPR accessibility parameter Π was calculated as previously described (*20*).

RESULTS

Twenty-six sequential cysteine mutants, spanning the sequence between P3 and T28 of the first transmembrane segment (TMS1) of EmrE, were constructed in a cysteine-less mutant of EmrE where the three native cysteines at residues 39, 41, and 95 were mutated to serines. The cysteine-less protein, hereafter referred to as WT*, has been shown to retain significant transport activity in vivo and in reconstituted proteoliposomes (*14*). Previous studies have shown that, except for a small subset of sites, a cysteine can be introduced at almost 50% of the residues in EmrE without debilitating effects on the structure or function of the protein (*14*). Remarkably, among the critically important residues, three are located in TMS1. E14 is highly conserved among members of the SMR family and is required for ligand binding to EmrE. As previously observed, residues 11 and 18 are within one helical turn of E14 and may also be associated with ligand binding (*14*). A mechanistic model of EmrE transport proposes a critical role of TMS1 in the formation of the transport pathway and the coupling of substrate and proton movements. Evidence in support of this interpretation based on the location of these residues near the binding site is presented below.

Of the 26 mutants reported in this paper, the transport activity of nine has been previously examined (*21*). Using an in vivo functional assay, we tested whether the cysteine mutants were able to confer resistance to ethidium. Except for residues 3, 4, 7, 10, 14, 18, and 22, the expression of the mutants allowed *E. coli* to grow in the presence of 200 μg/mL ethidium. As described below, the nonfunctional residues sequester on one side of TMS1 in the putative substrate binding pocket (Figure 4). Despite their effects on the function of EmrE, purified R1-labeled mutants have similar retention times to that of the WT on a SEC column, suggesting no change in their oligomeric structures.

TMS1 Is Located near a Subunit Interface. The room temperature EPR spectra of the R1-labeled EmrE mutants are shown in Figure 1. All spectra were recorded with a 100 G scan width except for E14R1 and T18R1, which were recorded at 250 and 200 G, respectively. Both spectra show distinct evidence of spin−spin interactions arising from nitroxides in close proximity. Because each EmrE subunit contains a single R1 side chain, the proximity must arise from the assembly of the subunits in the EmrE oligomer. Reconstitution of the E14R1 oligomer in the presence of excess WT* (see below) results in the disappearance of the spectral feature arising from spin−spin interactions as demonstrated by the light trace spectrum in Figure 1.

Furthermore, the spectrum of E14R1 reveals two distinct spectral components. The broad component, indicated by the arrows in Figure 1, is suggestive of a population of spins in very close proximity. The two external peaks, separated by more than 125 G, form a Pake doublet (*22*) and arise from transitions in a triplet state. In T4 lysozyme, a protein of known crystal structure, such spectra were observed in nitroxide pairs predicted by molecular modeling to be in van der Waals (VDW) contacts (*23*). The narrow component in the spectrum represents a minor population ($\approx$30%) where the spins are separated by a much larger distance ($\geq$20 Å).

The two-component spectrum of E14R1 can arise from underlabeling or the presence of protein contaminants or reflects a heterogeneous mixture of conformational states of EmrE. Despite the two-step purification and analysis of protein purity by SDS−PAGE, the presence of a protein contaminant is difficult to directly exclude since even a 5% level with multiple cysteines can have a substantial spectral contribution. To demonstrate that underlabeling is not at the origin of the complex spectrum of E14R1, spin concentration was determined using double integration and compared to a fresh sample of 4-hydroxy-Tempo. Absolute protein concentration, determined by amino acid analysis, indicates at least 95% labeling efficiency. This result is consistent with a comparable relative labeling efficiency at sites E14 and E25, the later being highly exposed to the aqueous solvent as demonstrated below. The EPR spectrum of E14R1 reconstituted in lipid vesicles was superimposable on that of Figure 1, thus excluding a detergent-induced destabilization of the oligomer as the origin of the two-component spectrum.

To determine the number of spins involved in the dipolar interaction, the dependence of the intensity of the Pake doublet high-field extremum on the addition of unlabeled WT* subunits was determined. To reconstitute the EmrE oligomer with added WT*, we used SDS as a denaturant at room temperature to dissociate the oligomer (*24*). Figure 2a shows the effects of various mole fractions of SDS on the EPR spectrum of E14R1. As SDS concentration increases, the intensities of the high- and low-field extrema, arising from spin−spin interactions, are reduced, demonstrating the dissociation of the oligomer. SDS denaturation is reversible; i.e., the broad spectral component can be regenerated upon removal of SDS (not shown). Therefore, various mixtures of E14R1 and WT* were co-denatured at 0.16 mole fraction of SDS, and then the complex was purified by SEC. As shown in panel b of Figure 2, there is a progressive decrease in the spectral features arising from the interacting spin population as the molar ratio of WT* to E14R1 is increased.

The dependence of the spectral amplitude on the amount of added WT* can be derived from the binomial distribution, assuming random reassembly of the EmrE oligomer from WT* and E14R1 subunits. The solid line in Figure 2c was computed on the basis of the assumption of a dimer. The close agreement with the experimental data demonstrates that the Pake doublet observed in the E14R1 spectrum arises from interactions between two R1 side chains around a 2-fold axis of symmetry.

Accessibility of TMS1 to Molecular Oxygen. To determine the secondary structure and the solvent accessibility profile of TMS1, the collision frequency of R1 with molecular oxygen and NiEDDA was measured at each site. Molecular oxygen is a nonpolar molecule that is preferentially soluble in hydrocarbon phases such as the interiors of micelles and membranes with increasing concentrations toward the middle of the micelle or the bilayer (*20*). Its solubility in water is limited while it is almost completely excluded from the packed protein interior. Thus, R1 scanning through aniso-

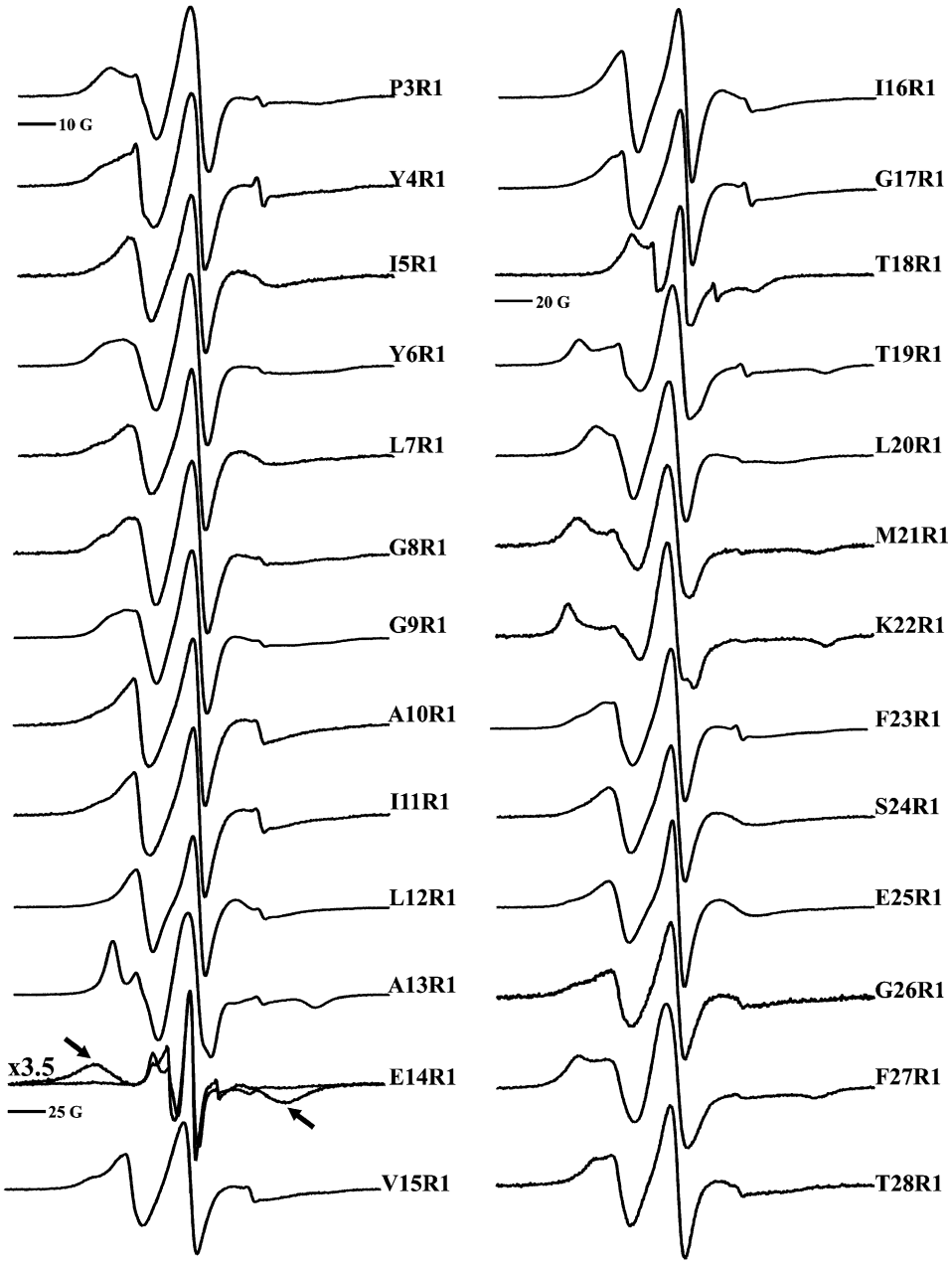

FIGURE 1: Room temperature EPR spectra of R1-labeled EmrE mutants in DM micelles. The spectra were normalized to represent the same number of spins and scaled for convenience of representation. All spectra were recorded with a 100 G scan width except E14R1 and T18R1, which were recorded with scan widths of 250 and 200 G, respectively. For E14R1, the thick line corresponds to the fully labeled mutant while the thin line corresponds to the mutant refolded with WT* at a ratio of 1:4. The fully labeled spectrum is scaled to show the details of the line shape.

tropically solvated segments of secondary structure should result in a periodic pattern in the accessibility profile of R1 to O_2 (*20*). Figure 3a shows such a periodic pattern in $\Pi(O_2)$, the EPR accessibility parameter, along TMS1. The periodicity is indicative of a regular α-helix particularly in the first half of TMS1, residues 3−15. Residues with maximum oxygen accessibility such as residues 5, 8, 12, and 16 face the micelle hydrocarbon phase while those with minimal $\Pi(O_2)$ are either water exposed or participate in tertiary contacts.

Superimposed on the rapid variation of $\Pi(O_2)$ in the first half of TMS1 is a slow increase in the absolute value of the local maxima, reflecting the progressively increased collision rates with O_2 expected for a transmembrane segment. In the second half of TMS1 the reverse behavior occurs with the value of the maximum $\Pi(O_2)$ decreasing. The change in Π is more abrupt in the residue 18−22 region where deviation from the 3.6 periodicity also occurs. Although residue 20 is at a local $\Pi(O_2)$ maximum, the value is lower than what is expected if the residue lies on the bilayer-exposed surface of a transmembrane helix. The origin of this effect is steric contacts along all of the faces of the helix as demonstrated by the mobility analysis below.

Accessibility of TMS1 to NiEDDA. The accessibility to NiEDDA, a reagent exclusively soluble in the aqueous phase, is reported in Figure 3b. Helical periodic behavior is only observed in the first eight residues. Furthermore, an abrupt increase in the accessibility to NiEDDA is observed at residues 25 and 26, indicating that these residues are at or beyond the micelle−water interface. There is no symmetric

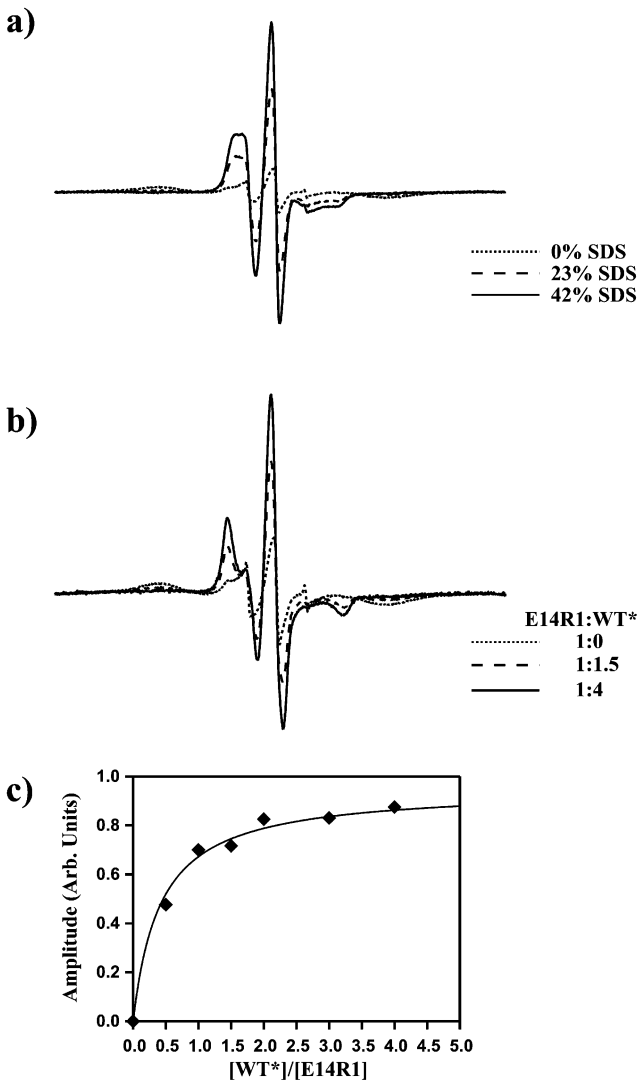

FIGURE 2: (a) EPR spectra of E14R1 in the presence of increasing amounts of SDS. All spectra were recorded with a 250 G scan width and were normalized to represent the same number of spins. The percentage of SDS represents the mole fraction of SDS in the total detergent concentration. (b) EPR spectra of E14R1 refolded in the presence of increasing amounts of WT* and 0.16 mole fraction of SDS. All spectra have a scan width of 250 G and are normalized to the same number of spins. (c) Increase in the fractional population of monomeric spins versus the molar ratio of WT*:E14R1. The solid line is the theoretical increase calculated from the binomial distribution assuming a dimeric interface.

residues with similar Π(NiEDDA) at the N-terminus of TMS1. Thus, it can be concluded that at residue 3 TMS1 is near or below the micelle−water interface.

R1 at residues identified as facing the micelle interior has no measurable exposure to NiEDDA, as expected on the basis of the lack of solubility of this reagent in the hydrocarbon phase. On the opposite side of the putative helix, R1 has significant accessibility to NiEDDA. This is particularly the case at sites 7, 10, 11, and 17. For comparison, Π(NiEDDA) for phospholipids spin labeled at positions 5 and 12 and incorporated into DM micelles are 0.139 and 0.117, respectively. Therefore, the sequence-specific change in Π(NiEDDA) in the first half of TMS1 arises from the sampling of at least two environments: one is exposed to the micelle hydrophobic interior while the other is in contact with the aqueous phase.

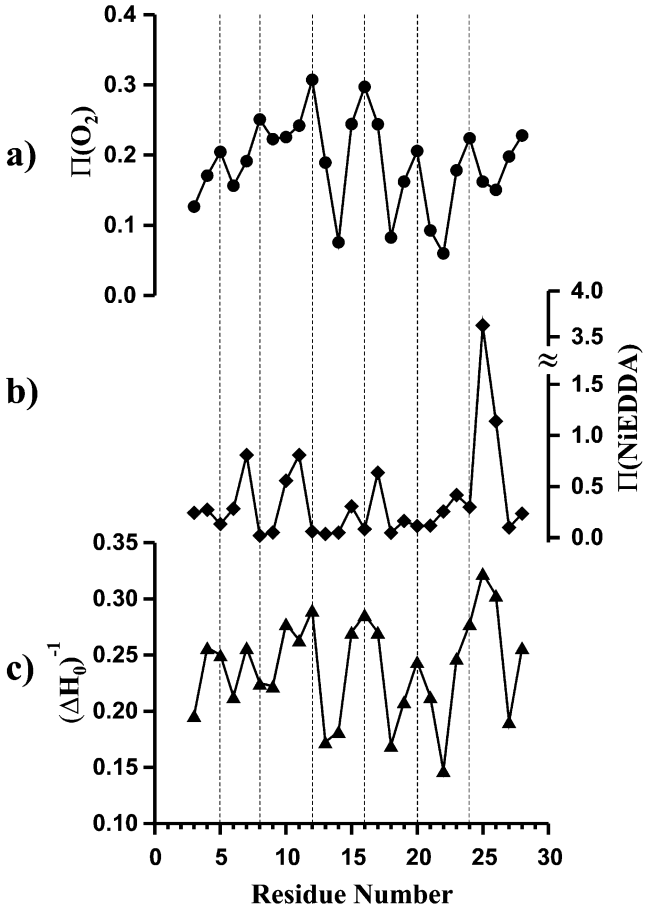

FIGURE 3: Accessibility and mobility profile of TMS1: (a) $\Pi(O_2)$, (b) Π(NiEDDA), and (c) $(\Delta H_0)^{-1}$ plotted versus residue number.

Similar to the $\Pi(O_2)$ profile, there is an overall decrease in the accessibility to NiEDDA in the residue 18−24 region, and the contrast between the various residues is minimal. The concomitant decrease in $\Pi(O_2)$ and Π(NiEDDA) further confirms a more strongly packed structure in this region.

Mobility of R1 across TMS1. The EPR spectra of Figure 1 show distinct spectral variations that reflect the mobility of R1 along TMS1. The major determinants of R1 mobility are the local steric constraints on the amplitude, rate, and geometry of R1 rotational isomerization (*25*). These constraints along TMS1 arise not only from the tertiary structure but also from contacts with another subunit across the 2-fold symmetric interface. Changes in mobility can be quantified using the inverse of the width of the central resonance line, $(\Delta H_0)^{-1}$, shown in Figure 3c as a function of residue number (*25*).

Between residues 3 and 20, the maximum in $(\Delta H_0)^{-1}$ occurs at the residues most exposed to O_2. In a transmembrane segment, such correspondence is expected at the residues facing the bilayer with no steric contacts with other regions of the protein. Consistent with this model, the EPR spectra at residues 10, 12, 16, and 17 reflect high mobility of the side chain R1. The plot of $(\Delta H_0)^{-1}$ also has a minimum between residues 18−22 precisely in the region of altered accessibility to O_2 and NiEDDA. Inspection of the EPR spectral line shape in Figure 1 suggests extensive steric constraints on the mobility of R1 in this region. Between residues 23 and 26, the EPR spectra are similar and indicate little, if any, restriction on mobility. This is in agreement

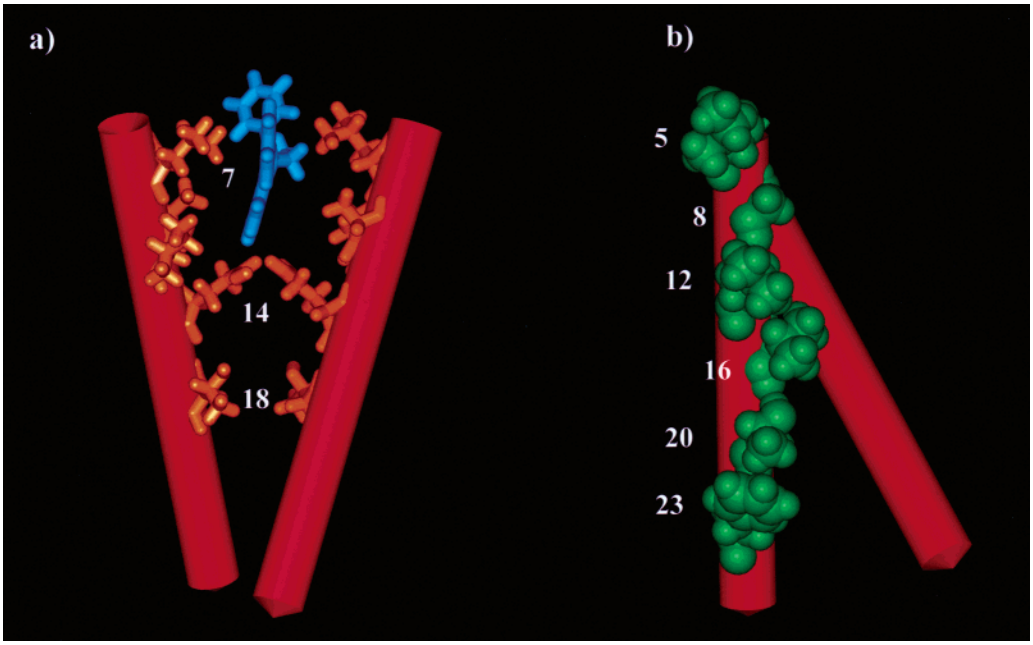

FIGURE 4: Molecular model of TMS1: (a) view of the substrate binding pocket with a bound ethidium molecule shown in blue; (b) side view showing residues facing the micelle.

with the increased Π(NiEDDA) in that region. Presumably, this turn of TMS1 starts near the micelle headgroup and emerges into the aqueous phase at residue 26.

DISCUSSION

Model of TMS1. The periodic variation in $\Pi(O_2)$ demonstrates that TMS1 has a helical conformation that extends from residue 3 to residue 24. The superimposed gradient of increasing accessibility, particularly in the first half of the helix, is consistent with a transmembrane configuration of the helix. The deviation from 3.6 periodicity in $\Pi(O_2)$ in the 18−23 region arises because of the contacts of this segment with other secondary structural elements in the oligomer and/or subunit contacts. Given the limited solubility of NiEDDA in the hydrocarbon phase, a continuous 3.6 periodicity in Π(NiEDDA) is not expected for a transmembrane helix unless the helix participates in a porelike structure with no physical barrier to diffusion (*20*).

Extensive broadening in the EPR spectral line shape of E14R1 and the dipolar splitting observed in T18R1 demonstrate that TMS1 from different subunits are in close proximity. The dimeric nature of EmrE is revealed in the dependence of the broadened spectral component on the ratio of WT* to labeled E14 and is in agreement with previous cryo-EM studies (*16*). That strong dipolar coupling is only detected at two sites suggests a specific model for the interaction between the two TMS1, as shown in Figure 4. The two TMS1 pack in a scissor-like fashion, bringing residues 14 and 18 into close proximity. On the basis of this model, nitroxides introduced at E14 are expected to pack in VDW contact while those introduced at T18 will be separated by a farther distance due to the off-axis location of T18 and the resulting projection of the nitroxides. In general, the model does not predict strong dipolar coupling (<15 Å) at other sites.

Figure 4 predicts a V-shaped chamber that is lined by TMS1 and possibly other secondary structural elements. Among the residues of TMS1 pointing toward the chamber are residues 7, 10, and 11. While room temperature spin−spin interaction is not detected between R1 at these sites, relatively weak broadening, expected from the model of Figure 4, may be averaged by the mobility around the nitroxide linking arm. Low-temperature spectral analysis can be used to measure the proximity of these residues and confirm this aspect of the model (*26*). Alternatively, the distances can be measured using pulsed EPR methods with a range of at least 50 Å (*27*).

Remarkably, residues 7, 10, and 11 have significant exposure to NiEDDA, suggesting that the chamber is accessible to the solvent. Solvent accessibility is also reflected in the mobile EPR spectra of R1 at these sites. The lack of motional restriction indicates that the side chains facing the chamber are not tightly packed. This allows for the binding of a substrate molecule such as ethidium, shown for the purpose of illustration in Figure 4. Furthermore, residues 7, 10, and 11 are hydrophobic, consistent with the chemical nature expected for the binding pocket (*28*, *29*). In support of this model, cysteine substitution at sites facing the chamber interior results in functionally impaired transporters, presumably due to interference with substrate binding.

The immobilized line shape at both residues 14 and 18, predicted also to face the binding chamber, suggests a possible protein barrier to passive diffusion. This results in a conelike shape for the chamber with extensive contact in the second part of the helix. While these contacts can account for the motional restriction of R1 at residues 18 and 22, the rather immobilized spectra at residues 13, 19, and 21 arise presumably due to tertiary interactions of TMS1 with other secondary structures in the oligomer or subunit. It is noted that a cone-shaped binding chamber has been observed in the transcriptional activator BMR (*30*) and in the ABC-multidrug transporter Msba (*31*).

Functional Implications. On the basis of a series of biochemical and mutagenic studies, Yerushalmi and Schul-

diner proposed a mechanistic model of the proton-coupled substrate translocation (*32*). In this model, E14 from different subunits is brought into close proximity in the oligomer, and the resulting charge cluster is part of the substrate binding pocket. A unique feature of this binding pocket is that it is shared by both protons and substrates. The occupancy is mutually exclusive in time, which provides a mechanism for coupling proton import to substrate extrusion.

The data presented in this paper lend support to the general outline of the model; in particular, the proximity of E14 confirms the electrostatic contribution to the transport process and is also in agreement with recent cross-linking data (*21*). Remarkably, the cross-linking efficiency at E14C is 50%, consistent with the observation that the spin population in close contact accounts for about 70% of the total spin population. This suggests that the origin of the two-component spectrum of E14R1 is the existence of a population of EmrE dimers where the two nitroxides are separated by >20 Å. Cryo-EM studies provide a hint of possible conformational heterogeneity in the EmrE dimer (*16*). Conformational flexibility is considered an intrinsic property of multidrug transporters and may be associated with their polyspecificity and transport.

ACKNOWLEDGMENT

The authors thank Neema Salimi for contribution to this work, in particular molecular modeling.

REFERENCES

1. Van Veen, H. W., and Konings, W. N. (1998) *Adv. Exp. Med. Biol. 456*, 145−158.
2. Gottesman, M. M., Fojo, T., and Bates, S. E. (2002) *Nat. Rev. Cancer 2*, 48−58.
3. Van Veen, H. W., Callaghan, R., Soceneantu, L., Sardini, A., Konings, W. N., and Higgins, C. F. (1998) *Nature 391*, 291−295.
4. Putman, M., Van Veen, H. W., Degener, J. E., and Konings, W. N. (2000) *Mol. Microbiol. 36*, 772−773.
5. Van Veen, H. W., and Konings, W. N. (1998) *Biochim. Biophys. Acta 1365*, 31−36.
6. Putman, M., Van Veen, H. W., and Konings, W. N. (2000) *Microbiol. Mol. Biol. Rev. 64*, 672−693.
7. Paulsen, I. T., Skurray, R. A., Tam, R., Saier, M. H., Jr., Turner, R. J., Weiner, J. H., Goldberg, E. B., and Grinius, L. L. (1996) *Mol. Microbiol. 19*, 1167−1175.
8. Yerushalmi, H., Lebendiker, M., and Schuldiner, S. (1995) *J. Biol. Chem. 270*, 6856−6863.
9. Muth, T. R., and Schuldiner, S. (2000) *EMBO J. 19*, 234−240.
10. Yerushalmi, H., and Schuldiner, S. (2000) *J. Biol. Chem. 275*, 5264−5269.
11. Schwaiger, M., Lebendiker, M., Yerushalmi, H., Coles, M., Groger, A., Schwarz, C., Schuldiner, S., and Kessler, H. (1998) *Eur. J. Biochem. 254*, 610−619.
12. Arkin, I. T., Russ, W. P., Lebendiker, M., and Schuldiner, S. (1996) *Biochemistry 35*, 7233−7238.
13. Edwards, R. A., and Turner, R. J. (1998) *Biochem. Cell Biol. 76*, 791−797.
14. Mordoch, S. S., Granot, D., Lebendiker, M., and Schuldiner, S. (1999) *J. Biol. Chem. 274*, 19480−19486.
15. Yerushalmi, H., Lebendiker, M., and Schuldiner, S. (1996) *J. Biol. Chem. 271*, 31044−31048.
16. Tate, C. G., Kunji, E. R., Lebendiker, M., and Schuldiner, S. (2001) *EMBO J. 20*, 77−81.
17. Hubbell, W. L., Mchaourab, H. S., Altenbach, C., and Lietzow, M. A. (1996) *Structure 4*, 779−783.
18. Berliner, L. J., Grunwald, J., Hankovszky, H. O., and Hideg, K. (1982) *Anal. Biochem. 119*, 450−455.
19. Yerushalmi, H., and Schuldiner, S. (2000) *FEBS Lett. 476*, 93−97.
20. Hubbell, W. L., Gross, A., Langen, R., and Lietzow, M. A. (1998) *Curr. Opin. Struct. Biol. 8*, 649−656.
21. Soskine, M., Steiner-Mordoch, S., and Schuldiner, S. (2002) *Proc. Natl. Acad. Sci. U.S.A. 99*, 12043−12048.
22. Pake, G. E. (1948) *J. Chem. Phys. 16*, 327−336.
23. Mchaourab, H. S., Oh, K. J., Fang, C. J., and Hubbell, W. L. (1997) *Biochemistry 36*, 307−316.
24. Lau, F. W., and Bowie, J. U. (1997) *Biochemistry 36*, 5884−5892.
25. Mchaourab, H. S., Lietzow, M. A., Hideg, K., and Hubbell, W. L. (1996) *Biochemistry 35*, 7692−7704.
26. Rabenstein, M. D., and Shin, Y. K. (1995) *Proc. Natl. Acad. Sci. U.S.A. 92*, 8239−8243.
27. Borbat, P. P., Mchaourab, H. S., and Freed, J. H. (2002) *J. Am. Chem. Soc. 124*, 5304−5314.
28. Godsey, M. H., Zheleznova Heldwein, E. E., and Brennan, R. G. (2002) *J. Biol. Chem. 277*, 40169−40172.
29. Zheleznova, E. E., Markham, P., Edgar, R., Bibi, E., Neyfakh, A. A., and Brennan, R. G. (2000) *Trends Biochem. Sci. 25*, 39−43.
30. Zheleznova, E. E., Markham, P. N., Neyfakh, A. A., and Brennan, R. G. (1999) *Cell 96*, 353−362.
31. Chang, G., and Roth, C. B. (2001) *Science 293*, 1793−1800.
32. Yerushalmi, H., and Schuldiner, S. (2000) *Biochemistry 39*, 14711−14719.

BI0342867